doi:10.5607/en.2011.20.1.45

Experimental Neurobiology
Vol. 20, pages 45~53, March 2011

Rapid Disruption of Cellular Integrity of Zinc-treated Astroglia Is Regulated by p38 MAPK and Ca^{2+}-dependent Mechanisms

Joo-Young Im[#], Hyo-Jin Joo[#] and Pyung-Lim Han*

Departments of Brain & Cognitive Sciences, and Chemistry & Nano Science, Ewha Womans University, Seoul 120-750, Korea

ABSTRACT

Cultured cortical primary astroglia treated with zinc died while rapidly detached from culture plates, a distinct part of zinc-treated astroglia. In the present study, we investigated the mechanism underlying the rapid change in the morphologic integrity of zinc-treated astroglia. Among the early cellular events occurring in zinc-treated astroglia, strong activation of p38 MAPK and JNK was evident. Although inhibitors of p38 (SB203580 and SB202190) or JNK (SP600125) did not protect zinc-insulted astroglia from cell death, the p38 inhibitors, but not the JNK inhibitor, suppressed actin filament and cell morphology disruption. The Ca^{2+} ionophore, A23187, also suppressed actin filament and cell morphology disruption, but not cell death, of zinc-insulted astroglia. However, A23187 did not inhibit p38 MAPK activation in zinc-treated astroglia. Together these results suggest that zinc influx in astroglia results in rapid loss of the morphologic integrity via mechanisms regulated by p38 kinase and/or Ca^{2+} signaling.

Key words: astroglia, zinc, morphology protection, p38 inhibitors, actin filament

INTRODUCTION

Acute pathologic conditions, such as cerebral ischemia, induce excess release of free zinc from excitatory synapses, and excessively released zinc causes brain cells to die (Frederickson et al., 2005). Zinc-induced cell death occurs via zinc influx into cells, and zinc influx results in disruption of thiol homeostasis and reactive oxygen species (ROS) stress (Frederickson et al., 1988; Kim et al., 1999a; 1999b; Suh et al., 2000; Kim et al., 2003). *In vitro* studies have shown that both neurons and astroglia are sensitive to chronic low doses of free zinc (Dineley et al., 2000; Cho et al., 2003; Ralph et al., 2010). Cultured primary astroglia cells challenged with free zinc become elongated in shape, swell and soon thereafter detach from the culture plate. The rapid change and characteristic loss of morphologic integrity of astroglia cells precedes with the events leading to cell death (Cho et al., 2003; Kim et al., 2003). Astroglial cell death induced by zinc is different from that of other insults, such as H_2O_2 or Fe^{2+}, in that astroglia cells treated with the latter stimulants undergo demise, while most cells are attached on the culture plate. Cell morphology changes, including detachment from the culture

[#]These authors equally contributed to this work.
*To whom correspondence should be addressed.
TEL: 82-2-3277-4130, FAX: 82-2-3277-3419
e-mail: plhan@ewha.ac.kr
Received December 20, 2010
Accepted for publication December 31, 2010

plate, might proceed with disruption of cytoskeletal elements. Because zinc-induced astroglia death is initiated by zinc-influx (Ryu et al., 2002; Kim et al., 2003), the rapid and distinct loss of morphologic integrity is likely to occur via zinc-mediated changes in dynamics of cytoskeletal elements. However, it is unclear how this process occurs and whether intracellular cytoskeleton dysregulation is a prerequisite to the cell death process in zinc-insulted cells.

Actin is the major cytoskeletal element in most eukaryotic cells. Failure of actin dynamics leads to disruption of cell morphology (Carlier et al., 1994; Dalle-Donne et al., 2001). Actin dynamics and cell morphology have been shown to be regulated by several factors, including mitogen-activated protein kinases (MAPKs). For instance, the MEK inhibitor, U0126, blocks stellate process extension of fibroblast growth factor 2 (FGF2)-treated astroglia *in vitro*, while inhibition of the p38 MAPK pathway by SB202190 facilitate stellate process growth and extension of the same cells (Heffron and Mandell, 2005). The p38 MAPK cascade regulates actin polymerization in platelet-derived growth factor-induced cytoskeleton remodeling of aortic smooth muscle cells (Pichon et al., 2004). p38 MAPK activation induces actin re-arrangements in VEGF-treated human endothelial cells (Rousseau et al., 1997). MAPK activated protein kinase 2 regulates actin polymerization in ventilator associated lung injury (Damarla et al., 2009).

Intracellular Ca^{2+} homeostasis is also important in the maintenance of cell morphology. Calcium stimulates actin filament assembly (Downey et al., 1990; Carlier et al., 1994), and Ca^{2+}-mediated actin filament regulation contributes to growth cone behaviors, synaptic vesicle trafficking in presynaptic terminals, and synaptic plasticity in dendritic spines of postsynaptic neurons (Matus, 2000; Levitan, 2008). Calcium also activates Ca^{2+}-dependent proteases, for examples calpains, that cleave actin-binding proteins, dissociating the anchorage between the plasma membrane and cytoskeleton (Harris and Morrow, 1990; Carragher and Frame, 2002).

MAPKs are important elements in neuronal and non-neuronal cell death (Wang et al., 1998; Guo and Bhat, 2007). Zinc influx stimulates MAPK pathways in neuronal cells (Seo et al., 2001; An et al., 2005). ERK1/2 signaling leads to mitochondrial dysfunction in extracellular zinc-induced neurotoxicity in rat cultured neurons (He and Aizenman, 2010). In the present study, we explored the mechanisms that underlie rapid changes in the morphologic integrity of zinc-treated astroglia.

MATERIALS AND METHODS

Primary neuronal and astroglial cultures

Primary cortical neuron and astroglia were cultured, as described previously (Cho et al., 2003; Im et al., 2006a). Primary cortical neuronal cultures were prepared from embryonic day 15.5 (E15.5) ICR mouse cortices. Mouse cortices were triturated and dissociated cortical cells were plated in minimal essential medium (MEM) supplemented with 20 mM glucose, 5% fetal bovine serum (FBS), 5% horse serum, and 2 mM glutamine, at a density of 5 hemispheres per plate (4×10^5 cells per well) onto poly-D-lysine (100 μg/ml) and laminin (4 μg/ml) coated 24-well plates. On day 6 *in vitro* (DIV6), cytosine arabinoside was added to a final concentration of 10 μM and maintained for 2 days to halt glial growth. FBS and glutamine were not supplemented in the culture medium from day 6, and the medium was changed twice a week after day 8. Cultures in DIV13-15 were used for studies. When treated with zinc and/or drugs, HEPES-buffered salt solution (120 mM NaCl, 5.4 mM KCl, 0.8 mM MgCl2, 1.8 mM CaCl2, 20 mM HEPES, 10 mM NaOH, and 15 mM glucose) was used.

Cortical astroglia cells were cultured, as described previously (Cho et al., 2003; Im et al., 2006b). ICR neonatal mice (day 0-1) were sacrificed and the cortices were isolated. Dissociated cortical cells were plated in MEM supplemented with 20 mM glucose, 5% fetal bovine serum, 5% horse serum, 2 mM glutamine, 50 μg/ml streptomycin, and 50 unit/ml penicillin at a density of 2 hemispheres per plate (5×10^4 cells per well) onto poly-D-lysine-coated (20 μg/ml) 24-well plates. Cells were maintained at 37°C in a humidified 5% CO_2 incubator. The medium was changed twice a week. The experiments were carried out on cells which were grown to confluence, and obtained after 2 weeks of culturing. Cortical astroglia cultures were characterized by anti-GFAP antibody (Dako, Carpinteria, CA, USA), an astrocyte marker, and isolectin B4

conjugated antibody (Sigma, St. Louis, MO, USA), a microglia marker, as described previously (Cho et al., 2003). Various inhibitors or drugs, including SB203580 and SB202190, were obtained from Calbiochem (La Jolla, CA, USA).

Western blot analysis

Western blot analysis was carried out as described previously (Im et al., 2006a). Briefly, primary astroglia were suspended in lysis buffer containing 150 mM NaCl, 1% NP-40, 0.1% SDS, 0.5% sodium deoxycholate, 1 mM phenylmethylsulfonyl fluoride (PMSF), 1 mM Sodium orthovanadate (Na_3VO_4), and protease inhibitor cocktails (Roche, Basel, Swiss) in 20 mM Tris-HCl (pH 7.4). Lysates were centrifuged for 10 min at 12,000 rpm at 4°C, and the resulting supernatants were collected. Protein contents were determined using a bicinchoninic acid assay kit (St. Louis, MO, USA). Protein samples were electrophoresed by 10% SDS-PAGE and then transferred to polyvinylidene difluoride membranes (Bio-Rad, Hercules, CA, USA). The blots were blocked with 5% non-fat dried milk for 1 h and incubated with primary antibodies overnight at 4°C. The secondary antibody was incubated for 1 h and specific signals were detected using an enhanced chemiluminescence (ECL) kit (Amersham, Buckinghamshire, UK). Immunoblotting was performed using polyclonal anti-phospho-p38 (1 : 1,000, Cell signaling, USA), polyclonal anti-phospho-JNK (1 : 1,000, Cell signaling, USA), polyclonal anti-p38 (1 : 1,000, Santa Cruz, CA, USA), and monoclonal anti-JNK1 (1 : 1,000, Pharmingen, USA).

Assessments of cell death

Cell death was assessed by measuring the activity of lactate dehydrogenase (LDH) released in culture medium as described previously (Im et al., 2006a). Culture medium was collected 24 h after drug treatment to use for LDH activity unless indicated otherwise. Twenty-five μl of culture medium was transferred to a microplate and 100 μl of NADH solution (0.3 mg/ml NADH and 0.1 M potassium phosphate, pH 7.4) was added to the medium. Subsequently after 2 min, 25 μl of pyruvate solution (22.7 mM pyruvate and 0.1 M potassium phosphate, pH 7.4) was added. After adding pyruvate solution, the decrease of absorbance at 340 nm, which indicates the conversion of NADH to NAD^+, was measured by SpectraMax microplate reader (Molecular Device, Sunnyvale, USA). LDH activity was normalized in that sham-treated culture and culture showing complete cell death were 0% and 100%, respectively, and normalized LDH activity was regarded as an indicator of cell death. Complete cell death was induced by treatment of cells to 2 mM H_2O_2 for 24 h. Cell death was also confirmed by trypan blue staining, and by morphological changes on phase contrast microscope.

Immunofluorescence-labeled phalloidin staining of F-actin

Visualization of actin filament distribution in cells was performed as described previously (Chae et al., 2006). Cortical cells were fixed by 4% paraformaldehyde solution for 10 min at room temperature and washed in PBS twice. Then the cells were treated with 0.5% triton X-100 in PBS to help penetration of phalloidin. After being washed, the cells were stained with 0.4 μg/ml phalloidin-TRITC (Sigma, St Louis, MO, USA) for 90 min at 4°C. Stained cells were photographed by fluorescence light microscope (Axiovert 200, Carl Zeiss Micro-Imaging, Inc., USA).

Statistical analysis

All data were analyzed using Student *t*-test for comparisons between two samples or using ANOVA followed by the Newman-Keuls test. A statistical difference was accepted at 5% level.

RESULTS

Zinc-treated astroglia showed strong activation of p38 and JNK MAPKs

Astroglial cells insulted with zinc were elongated in shape after 6 h, then gradually swelled and detached from the bottom of culture plate after 9 h. The rapid loss of morphological integrity in zinc-treated cells proceeded in parallel with the cellular process leading to cell death as demonstrated in previous studies (Cho et al., 2003; Kim et al., 2003). To understand the mechanism underlying the extraordinarily rapid changes in cell's integrity and cell death processes of zinc-treated cells, we tested whether p38 and JNK were involved. As

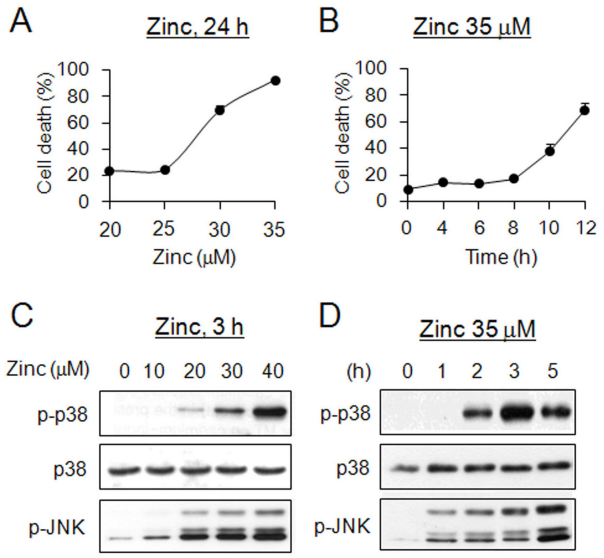

Fig. 1. p38 and JNK MAPKs were activated in zinc-treated astroglia. (A, B) Astroglial cell death by zinc increased in a zinc-dose (A) and zinc- treated time (B) dependent manner. LDH assay was performed after 24 h-exposure of cultures to indicated concentrations of zinc. (C) Western blots showing zinc-dose dependent activation of p38 and JNK MAPKS in astroglia. Assay was performed 3 h after zinc treatment. Anti-phospho- p38 MAPK and anti-phospho-JNK were used to deduce the activation levels of these kinases. (D) Western blots showing time-dependent activation of p38 and JNK MAPKS in zinc (35 μM)-treated astroglia.

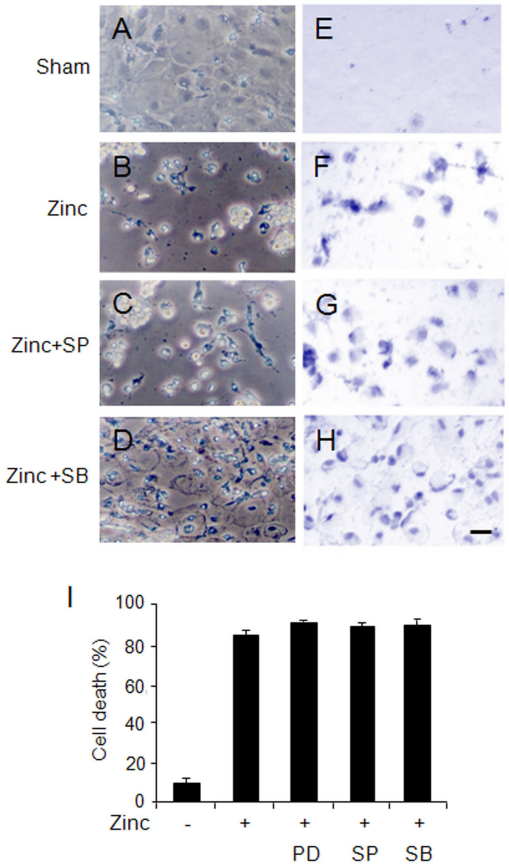

Fig. 2. The p38 MAPK inhibitor, SB203580, suppressed zinc-induced morphology disruption and detachment from the culture plate. (A～H) Phase contrast (A～D) or trypan-blue stained (E～H) astroglia with sham treatment (A, E) or astroglia treated with zinc (B, F), with zinc and SP600125 (C, G), or with zinc and SB203580 (D, H). Photomicrographs were taken 24 h after zinc (35 μM)-treatment in the presence of SP600125 (20 μM) or SB203580 (20 μM). Scale bar represents 100 μm. (I) LDH assay showing cell death levels of zinc (35 μM)-treated astroglia in the presence of PD98059 (PD: 20 μM), SP600125 (SP: 20 μM), or SB203580 (SB: 20 μM). LDH assay was performed 24 h after zinc treatment.

reported previously (Cho et al., 2003; Kim et al., 2003), zinc-dose and zinc-treated time dependent astroglial deaths were observed (Fig. 1A and B). Western blot analysis using anti-phospho-p38 or anti-phospho-JNK showed that both MAPKs were activated in 3 h after zinc challenge in a zinc-dose dependent manner (Fig. 1C). The activation of p38 MAPK by zinc (35 μM) was maximal at ～3 h after zinc challenge, and thereafter were slowly declined (Fig. 1D).

p38 MAPK inhibitors suppressed cell morphology disruption of zinc-insulted astroglia

We examined whether p38 and JNK MAPKs were critical players in zinc-induced astroglia death. Addition of p38 MAPK inhibitors, SB202190 or SB203580, in culture media had zinc-treated astroglia on the culture plate with a complete attachment. Moreover, zinc-treated astroglia appeared intact in the presence of SB203580 when examined by a phase-contrast microscopy (Fig. 2A～D). However, it was not the case. The zinc-challenged SB203580-cotreated astroglia cells were strongly stained by trypan-blue (Fig. 2E～H), suggesting that they were not alive. Indeed, LDH assay showed that SB203580 and SB202190 did not protect from cell death of zinc-treated astroglia (Fig. 2I). Neither the JNK inhibitor, SP600125, nor the MEK inhibitor, PD98059, produced protective effects on zinc-induced cell death and cell morphology disruption (Fig. 2I; Table 1).

The treatment of primary astroglia with Cd^{2+} (10 μM) or H_2O_2 (300 μM) also activated p38 MAPK and caused to cell death (data not shown). However, SB203580 did not prevent both morphological

Table 1. Effects of various cellular factor inhibitors on morphological disruption and cell death of zinc-treated astroglia

Inhibitors	Concentration	Effects	
		Death protection	Morphology protection
Potein kinase inhibitors			
PD98059	10～20 μM	No	No
SP600125	1～20 μM	No	No
SB203580	1～20 μM	No	Yes
SB202190	0.1～20 μM	No	Yes
GFX	1～3 μM	No	No
H89	1 μM	No	No
KN62	1 μM	No	No
Phosphatase inhibitors			
OKA	1 μM	No	No
Antioxidants			
NS398	30～100 μM	No	No
DPI	1～10 μM	No	No
Allopurinol	1～5 mM	No	No
PBN	200～500 μM	No	No
NAME	1～5 mM	No	No
PDTC	25～100 μM	No	No
NDGA	10～100 μM	No	Yes
Caspase inhibitor			
ZVAD	10～30 μM	No	No
PARP inhibitor			
Benzimide	1～5 mM	No	No
Ca^{2+} regulator			
A23187	0.1～1 μM	No	Yes

Assays were performed 24 h after Zn^{2+} (35 μM)-treatment. Inhibitors were applied to cultures 1 h prior to the start of Zn^{2+} treatment

Table 2. Effects of the p38 MAPK inhibitor, SB203580, on morphological disruption and cell death of zinc-treated C6 glioma and NIH3T3 cells

Cell types	Zinc concentration	Death protection	Morphology protection
Primary astroglia	35 μM	No	Yes
C6 glioma	35 μM	No	No
NIH3T3	20 μM	No	No

Assays were performed 24 hrs after Zn^{2+} treatment. SB203580 was applied to cultures 1 h before Zn^{2+} treatment. *SB203580 concentration was 20 μM.

Table 3. Effects of the p38 MAPK inhibitor, SB203580, on morphological disruption and cell death of H_2O_2- or cadmium-treated primary astroglia culture

Stimuli	Concentration	Death protection	Morphology protection
$ZnSO_4$	35 μM	No	Yes
H_2O_2	300 μM	No	Yes
Cadmium	10 μM	No	No

Assays were performed 24 hrs after Zn^{2+} treatment. SB203580 was applied to cultures 1 h before Zn^{2+} treatment. *SB203580 concentration was 20 μM

disruption and cell death induced by Cd^{2+} or H_2O_2 (Table 2). In addition, SB203580 did not suppress morphological disruption and cell death of zinc (100 μM)-treated C6 glioma cells and of zinc (100 μM)-treated NIH3T3 fibroblasts (Table 3). These results raise the possibility that SB203580-dependent morphological protection is a process that is a distinct property of zinc-treated primary astroglia.

Supplement of intracellular Ca^{2+} helped the maintenance of cell morphology of zinc-insulted astroglia

We searched for other cellular signaling pathways that produce morphological disruption of zinc-treated astroglia. Inhibitors of ROS generating enzymes, namely the COX-2 inhibitor NS398 (30 μM), the NADPH oxidase inhibitor DPI (1 μM), the xanthine oxidase inhibitor allopurinol (5 μM), and the NOS inhibitor N-nitro-l-arginine methyl ester (L-NAME) (1 mM), and the free radical trapping agent phenyl-alpha-tert-butyl nitrone (PBN) (200 μM) did not affect zinc-induced morphological changes. In addition, the caspase inhibitor zVAD (10 μM), the PARP inhibitor benzamide (1 mM), the protein phosphatase 2A inhibitor okadaic acid (OKA; 1 μM), the NF-κB inhibitor pyrrolidine dithiocarbamate (PDTC; 100 μM), protein kinase-A inhibitor H89 (1 μM), the Ca^{2+}-calmodulin-dependent protein kinase (CAMK) inhibitor KN62 (1 μM), and the protein kinase C (PKC) inhibitor GF109203X (GFX; 1 μM) were also ineffective (Table 1).

Next, we examined whether cell morphology of zinc-treated astroglia can be regulated by Ca^{2+}. Co-treatment of astroglia with A23187 (0.1 μM), a Ca^{2+} ionophore, for 24 h did not inhibit zinc-induced cell death (Fig. 3A), but did suppress cell morphology disruption, thus leaving zinc-treated cells attached on the culture plate (Fig. 3B～E). Treatment with the Ca^{2+} chelator, BAPTA (10 μM) suppressed cell morphology disruption and partially cell death of zinc-insulted astroglia (Fig. 3F～L). Together, these results suggest that Ca^{2+} is important for the maintenance of cell morphology of

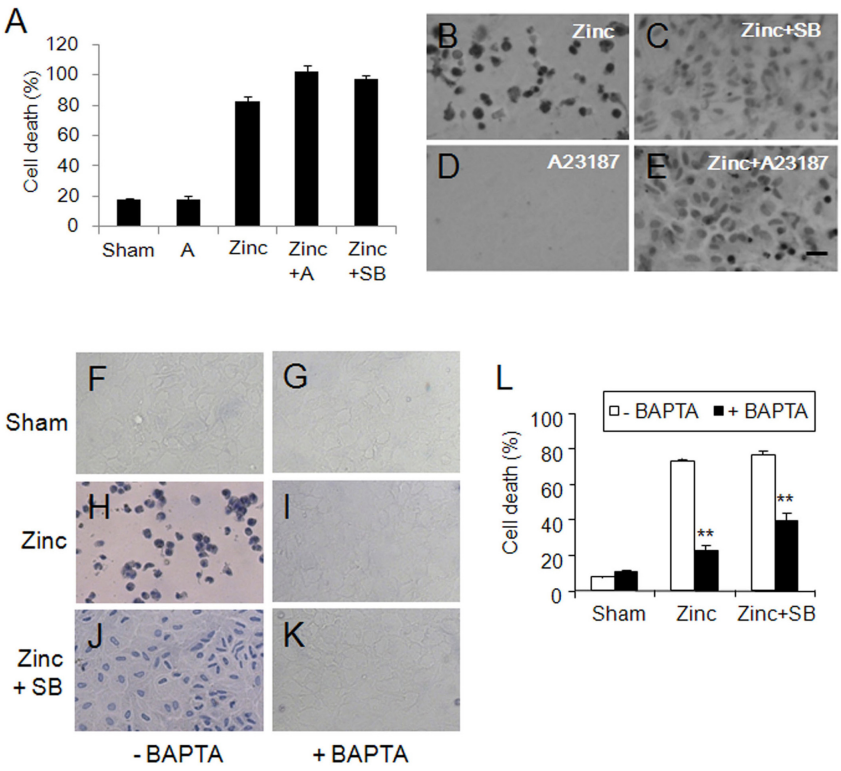

Fig. 3. The Ca^{2+} ionophore, A23187, suppressed cell morphology disruption of zinc-treated astroglia. (A) LDH assay showing cell death levels of astroglia treated with A23187 (0.1 μM), zinc (35 μM), zinc (35 μM)+A23187 (0.1 μM), or zinc (35 μM)+SB203580 (20 μM). LDH assay was performed after 24 h of drug treatment. (A) A23187; SB, SB203580. (B~E) Trypan-blue stained astroglia treated with zinc (35 μM), zinc (35 μM)+SB203580 (20 μM), A23187 (0.1 μM) or zinc (35 μM)+A23187. Photomicrographs were taken after 24 h of zinc treatment in the presence of SB203580 or A23187. (F~K) Trypan-blue stained astroglia with sham treatment (F, G), with zinc (H, I), or with zinc and SB203580 (J, K) in the presence or absence of the Ca^{2+} chelator, BAPTA (10 μM). Photomicrographs were taken 24 h after treatment of zinc (35 μM) and SB203580 (20 μM). (L) LDH assay showing cell death levels of astroglia treated with zinc (35 μM) or zinc (35 μM)+SB203580 (20 μM) in the presence or absence of BAPTA (10 μM). LDH assay was performed after 24 h of drug treatment. Scale bar represents 100 μm. SB, SB203580. The data are presented as means ±S.E.M. (n=6~12). **Denotes difference at $p < 0.05$.

zinc-insulted astroglia.

Zinc influx disrupted actin filament organization in astroglia, which was reversed by p38 inhibitors or A23187

Because cell morphology of zinc-treated astoglia was retained in the presence of SB203580 or A23187, we extended our efforts to visualize the actin organization in zinc-treated astoglia. Zinc-treated astoglia were stained with TRITC-conjugated phalloidin which labels actin fibers. Microscopic examination revealed that actin fibers in untreated normal astroglia were distributed throughout the cytoplasm, along with a mildly preferential localization at the plasma membrane. After 9~10 h of zinc treatment, actin filament distribution in the cytoplasm was disorganized by leaving numerous patched clumps within cells. However, in the presence of SB203580, zinc-induced actin filament disruption disappeared, and instead preferential distribution of actin filament at the cell periphery was strongly reinforced, giving rise to a distinct actin filament-ring along the plasma membrane (Fig. 4A~C).

Because the Ca^{2+} ionophore, A23187, also maintained cell morphology of zinc-insulted astroglia (Fig. 3B), we examined whether A23187 stabilized actin filament organization. Phalloidin-staining of zinc-treated astroglia showed that A23187 (0.1 μM) protected actin filament disruption of zinc-treated astroglia so that the resulting actin filament distribution was indistinguishable from that displayed by untreated astroglia. A23187 did not produce actin-ring formation along the plasma membrane (Fig. 4).

Next, we tested whether Ca^{2+}-mediated process acts over the p38 MAPK pathway in zinc-insulted astroglia. Western blot data showed that A23187 did not suppress p38 MAPK activation in zinc-treated astroglia (Fig. 5). These results suggest that Ca^{2+}-mediated process is not in the up-stream of p38 MAPK-mediated process.

DISCUSSION

The present study demonstrates that the Ca^{2+} ionophore A23187 and the p38 MAPK inhibitors (SB203580 and SB202190) suppressed rapid cell morphology disruption that distinctly occurs in zinc-treated astroglia. These results suggest that

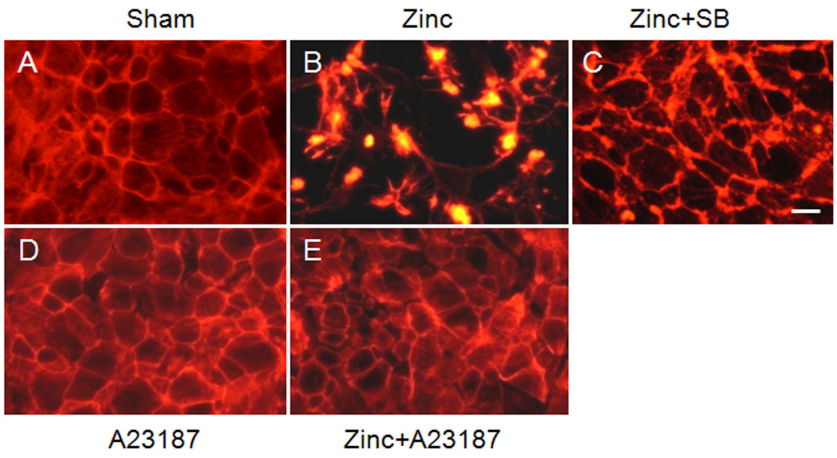

Fig. 4. SB203580 and A23187 suppressed actin-filament disruption in zinc-treated astroglia. (A~E) Photomicrographs showing actin-filament distributions in zinc-treated astroglia stained with TRITC-labeled phalloidin. Sham control (A) and astroglia treated with Zn (35 μM) alone (B), Zn (35 μM)+SB203580 (20 μM) (C), A23187 (0.1 μM) alone (D), or zinc (35 μM)+A23187 (0.1 μM) (E). Actin-filament disruptions were visualized after 10 h of zinc treatment. Scale bar represents 100 μm.

Ca^{2+} signaling and/or the p38 MAPK pathway are mechanism(s) that regulate actin filament dynamics in zinc-treated astroglia. A23187 produced a completely protection of cell morphology and actin-filament stabilization in zinc-treated astroglia, whereas SB203580 produced similar stabilization effects with leaving abnormally intensified actin filament-ring formation along the cell membrane, suggesting that in zinc-insulted astroglia, zinc influx-induced disturbance of cell morphology might be diverse.

The present study demonstrates that supplement of Ca^{2+} into zinc-treated astroglia using the Ca^{2+} ionophore, A23187, protected cell morphology disruption of zinc-treated astroglia. Therefore, we speculate that zinc influx disrupts Ca^{2+} homeostasis or Ca^{2+} availability in zinc-treated astroglia, which in turns affects actin filament destabilization, resulting in rapid loss of the morphological integrity. Disruption of Ca^{2+} availability or substitution of Ca^{2+} by Zn^{2+} might affect the function of Ca^{2+}-dependent proteases or Ca^{2+} regulating factors such as calreticulin and calbibdin. For examples, calpains are Ca^{2+}-dependent proteases that cleave actin-binding proteins (Harris and Morrow, 1990; Carragher and Frame, 2002). Calreticulin potentially has a role in cell adhesion and maintenance of intracellular Ca^{2+} homeostasis (Michalak et al., 1998). Zinc influx induces functional disruption of thiol-containing cellular factors (Frederickson et al., 1988; Kim et al., 2003) and increase of ROS stress (Kim et al., 1999a; 1999b; Suh et al., 2000). Our results add the evidence that zinc influx in astroglia causes a disturbance of Ca^{2+} homeostasis.

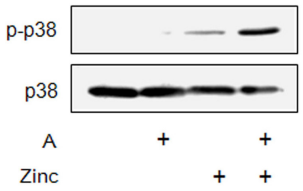

Fig. 5. A23187 did not suppress p38 MAPK activation in zinc-treated astroglia. Western blots showing p38 MAPK activation levels in zinc-treated astroglia. Western blot analysis was performed after 3 h of treatment with zinc (40 μM) alone or zinc (40 μM)+A23187 (A: 0.1 μM).

Concerning the effects of SB203580 on cell morphology and actin filament dynamics, it may be possible that the p38 MAPK pathway normally plays an inhibitory role in actin filament stabilization in zinc-treated astroglia. The notion that inhibition of p38 MAPK pathway by SB203580 enhances actin filament stabilization is consistent with the previous report that inhibition of the p38 MAPK pathway by SB202190 facilitated stellate process growth and extension of FGF2-treated primary astroglia (Heffron and Mandell, 2005). Stellate process extension of astroglia is an important aspect of reactive astrogliosis that occurs in a variety of pathological stimuli including trauma, ischemia, and neurodegenerative diseases (Chen and Swanson, 2003; Pekny and Nilsson, 2005). During the changes of stellate process extension of astroglia, actin filament breakdown, reassembly and stabilization should take place rapidly. Consistent with this view, reactive astrogliosis express high levels of p38 MAPK (Che et al., 2001; Piao et al., 2003). Many brain tumors arise from astoglia and metastasis of brain tumors

may undergo a phase in which cell adhesion and cell morphology changes are critical steps. The results of the present study may raise the possibility that the p38 MAPK pathway is an important regulator of morphological behaviors of brain cells with an astroglia-origin.

A23187 did not suppress p38 MAPK activation in zinc-treated astroglia and both factors distinctly regulate actin-filament organization. Therefore, we speculate that SB203580/SB202190 target(s) and Ca^{2+} signaling players independently work to stabilize cell morphology. Cell morphology preservation of zinc-treated astroglia by SB203580 and SB202190 is likely produced by stabilization of actin-filament organization by inhibiting p38 MAPK. However, we do not rule out the possibility that SB203580/SB202190 targets unidentified cellular factors regulating actin-filament organization. Our preliminary data showed that cell morphology stabilization, but no cell death protection, of zinc-treated astroglia can be also achieved by NDGA (nordihydroguaiaretic acid), which possess a lipoxygenase (LOX) inhibition activity and an anti-oxidant property (Konno et al., 1990; Arteaga et al., 2005), and causes GSH depletion (Im and Han, 2007). Regarding that A23187, SB202190 and NDGA might distinctly work within cells, the possibility that they may act on a common pathway still remains to be explored further in the future.

ACKNOWLEDGEMENTS

This research was supported by a grant (2010-K000814) from Brain Research Center, The 21st Century Frontier Research Program of the Ministry of Education, Science and Technology, Republic of Korea.

REFERENCES

An WL, Bjorkdahl C, Liu R, Cowburn RF, Winblad B and Pei JJ (2005) Mechanism of zinc- induced phosphorylation of p70 S6 kinase and glycogen synthase kinase 3beta in SH-SY5Y neuroblastoma cells. *J Neurochem* 92:1104-1115.

Arteaga S, Andrade-Cetto A and Cardenas R (2005) Larrea tridentata (creosote bush), an abundant plant of Mexican and U.S. American deserts and its metabolite nordihydroguaiaretic acid. *J Ethnopharmacol* 98:231-239.

Carlier MF, Valentin-Ranc C, Combeau C, Fievez S and Pantoloni D (1994) Actin polymerization: regulation by divalent metal ion and nucleotide binding, ATP hydrolysis and binding of myosin. *Adv Exp Med Biol* 358:71-81.

Carragher NO and Frame MC (2002) Calpain: a role in cell transformation and migration. *Int J Biochem Cell Biol* 34: 1539-1543.

Chae HJ, Ha HY, Im JY, Song JY, Park S and Han PL (2006) JSAP1 is required for the cell adhesion and spreading of mouse embryonic fibroblasts. *Biochem Biophys Res Commun* 345:809-816.

Che Y, Yu YM, Han PL and Lee JK (2001) Delayed induction of p38 MAPKs in reactive astrocytes in the brain of mice after KA-induced seizure. *Brain Res Mol Brain Res* 94: 157-165.

Chen Y and Swanson RA (2003) Astrocytes and brain injury. J Cereb *Blood Flow Metab* 23:137-149.

Cho YM, Bae SH, Choi BK, Cho SY, Song CW, Yoo JK and Paik YK (2003) Differential expression of the liver proteome in senescence accelerated mice. *Proteomics* 3: 1883-1894.

Dalle-Donne I, Rossi R, Milzani A, Di Simplicio P and Colombo R (2001) The actin cytoskeleton response to oxidants: from small heat shock protein phosphorylation to changes in the redox state of actin itself. *Free Radic Biol Med* 31:1624-1632.

Damarla M, Hasan E, Boueiz A, Le A, Pae HH, Montouchet C, Kolb T, Simms T, Myers A, Kayyali US, Gaestel M, Peng X, Reddy SP, Damico R and Hassoun PM (2009) Mitogen activated protein kinase activated protein kinase 2 regulates actin polymerization and vascular leak in ventilator associated lung injury. *PLoS One* 4:e4600.

Dineley KE, Scanlon JM, Kress GJ, Stout AK and Reynolds IJ (2000) Astrocytes are more resistant than neurons to the cytotoxic effects of increased [Zn (2+)] (i). *Neurobiol Dis* 7:310-320.

Downey GP, Chan CK, Trudel S and Grinstein S (1990) Actin assembly in electropermeabilized neutrophils: role of intracellular calcium. *J Cell Biol* 110:1975-1982.

Frederickson CJ, Hernandez MD, Goik SA, Morton JD and McGinty JF (1988) Loss of zinc staining from hippocampal mossy fibers during kainic acid induced seizures: a histofluorescence study. *Brain Res* 446:383-386.

Frederickson CJ, Koh JY and Bush AI (2005) The neurobiology of zinc in health and disease. *Nat Rev Neurosci* 6:449-462.

Guo G and Bhat NR (2007) p38alpha MAP kinase mediates hypoxia-induced motor neuron cell death: a potential target of minocycline's neuroprotective action. *Neurochem Res* 32:2160-2166.

Harris AS and Morrow JS (1990) Calmodulin and calcium-dependent protease I coordinately regulate the interaction of fodrin with actin. *Proc Natl Acad Sci USA* 87:3009-3013.

He K and Aizenman E (2010) ERK signaling leads to mitochondrial dysfunction in extracellular zinc-induced neurotoxicity. *J Neurochem* 114:452-461.

Heffron DS and Mandell JW (2005) Opposing roles of ERK and p38 MAP kinases in FGF2-induced astroglial process extension. *Mol Cell Neurosci* 28:779-790.

Hyrc KL, Bownik JM and Goldberg MP (2000) Ionic selectivity of low affinity ratiometric calcium indicators: mag-fura-2, fura-2FF and BTC. *Cell Calcium* 27:75-86.

Im JY and Han PL (2007) Nordihydroguaiaretic acid induces

astroglial death via glutathione depletion. *J Neurosci Res* 85:3127-3134.

Im JY, Kim D, Paik SG and Han PL (2006a) COX-2 dependent neuronal death proceeds via superoxide anion generation. *Free Radic Biol Med* 41:960-972.

Im JY, Paik SG and Han PL (2006b) Cadmium-induced astroglial death proceeds via glutathione depletion. *J Neurosci Res* 83:301-308.

Kim D, Joe CO and Han PL (2003) Extracellular and intracellular glutathione protects astrocytes from Zn^{2+}-induced cell death. *Neuroreport* 14:187-190.

Kim EY, Koh JY, Kim YH, Sohn S, Joe E and Gwag BJ (1999a) Zn^{2+} entry produces oxidative neuronal necrosis in cortical cell cultures. *Eur J Neurosci* 11:327-334.

Kim YH, Kim EY, Gwag BJ, Sohn S and Koh JY (1999b) Zinc-induced cortical neuronal death with features of apoptosis and necrosis: mediation by free radicals. *Neuroscience* 89:175- 182.

Konno C, Lu ZZ, Xue HZ, Erdelmeier CA, Meksuriyen D, Che CT, Cordell GA, Soejarto DD, Waller DP and Fong HH (1990) Furanoid lignans from Larrea tridentata. *J Nat Prod* 53:396-406.

Levitan ES (2008) Signaling for vesicle mobilization and synaptic plasticity. *Mol Neurobiol* 37:39-43.

Matus A (2000) Actin-based plasticity in dendritic spines. *Science* 290:754-758.

Michalak M, Mariani P and Opas M (1998) Calreticulin, a multifunctional Ca^{2+} binding chaperone of the endoplasmic reticulum. *Biochem Cell Biol* 76:779-785.

Pekny M and Nilsson M (2005) Astrocyte activation and reactive gliosis. *Glia* 50:427-434.

Piao CS, Kim JB, Han PL and Lee JK (2003) Administration of the p38 MAPK inhibitor SB203580 affords brain protection with a wide therapeutic window against focal ischemic insult. *J Neurosci Res* 73:537-544.

Pichon S, Bryckaert M and Berrou E (2004) Control of actin dynamics by p38 MAP kinase - Hsp27 distribution in the lamellipodium of smooth muscle cells. *J Cell Sci* 117: 2569-2577.

Rousseau S, Houle F, Landry J and Huot J (1997) p38 MAP kinase activation by vascular endothelial growth factor mediates actin reorganization and cell migration in human endothelial cells. *Oncogene* 15:2169-2177.

Ralph DM, Robinson SR, Campbell MS and Bishop GM (2010) Histidine, cystine, glutamine, and threonine collectively protect astrocytes from the toxicity of zinc. *Free Radic Biol Med* 49:649-657.

Ryu R, Shin Y, Choi JW, Min W, Ryu H, Choi CR and Ko H (2002) Depletion of intracellular glutathione mediates zinc-induced cell death in rat primary astrocytes. *Exp Brain Res* 143:257-263.

Seo SR, Chong SA, Lee SI, Sung JY, Ahn YS, Chung KC and Seo JT (2001) Zn^{2+}-induced ERK activation mediated by reactive oxygen species causes cell death in differentiated PC12 cells. *J Neurochem* 78: 600-610.

Suh SW, Chen JW, Motamedi M, Bell B, Listiak K, Pons NF, Danscher G and Frederickson CJ (2000) Evidence that synaptically released zinc contributes to neuronal injury after traumatic brain injury. *Brain Res* 852:268-273.

Wang Y, Huang S, Sah VP, Ross J Jr, Brown JH, Han J and Chien KR (1998) Cardiac muscle cell hypertrophy and apoptosis induced by distinct members of the p38 mitogen-activated protein kinase family. *J Biol Chem* 273: 2161-2168.